Experimental Study of a Retrofitted Scroll Compressor for operation with Two-phase Refrigerant Flows⋆

Nicolas Leclercq[a,*], Benedikt G. Bederna[b] and Vincent Lemort[a]

[a]Thermodynamics Laboratory, University of Liège, 4000, Liège, Belgium
[b]Schaufler Chair of Refrigeration, Cryogenics and Compressor Technology, Dresden University of Technology, 01069, Dresden, Germany

ARTICLE INFO

Keywords:
Two-phase compression
Scroll compressor
Experimental testing
Oil-refrigerant mixture
Mixture properties

ABSTRACT

The present paper introduces an experimental investigation of a scroll compressor working with two-phase refrigerant flows, in the frame of a novel thermodynamic cycle making use of two-phase compressions/expansions called REGEN-BY-2.

The design of the test bench dedicated to two-phase compression will first be explained. The objective of this test bench is to assess the performances of the compressor working with a two-phase refrigerant-oil mixture under varying conditions such as inlet pressures, inlet vapor qualities, oil circulation ratios, pressure ratios and speeds. Three experimental campaigns have been conducted, the first two are dedicated to compare different oils, while the third does not use any oil, thereby experimenting a pure-refrigerant two-phase compression. The methodology to obtain the compressor inlet vapor quality is detailed, and the related assumptions developed. The performance indicators, i.e., isentropic and volumetric efficiencies, are defined for a two-phase oil-refrigerant mixture. A total of 253 operating points (with and without oil) have been used to generate 3D maps, showing the evolution of the efficiencies for varying pressure ratios and inlet qualities. The results shows a decrease of efficiency at low vapor qualities, especially at high pressure ratios, where under-compression is amplified. Finally, the results of the pure-refrigerant compression are analyzed, showing decent isentropic efficiencies, with a minimum of 50% at a vapor quality of 0.35 and an optimal pressure ratio of 2.7.

1. Introduction

Two-phase compression can be categorized into two parts: on one hand, two different fluids can be used (e.g., air-water mixture or oil-refrigerant mixture), on the other hand, the state of one single fluid can be located under the saturation bell resulting in the presence of a liquid phase and a vapor phase. In some particular cases, a two- or three- component zeotropic mixture can be used, where each component can be found in both liquid and vapor phases with different fractions. In the former case, experimental studies have started in the nineteen fifties, where the use of oil to lubricate air screw compressors was necessary to expand machines lifetime and improve machine performance of the Lysholm turbine, using timing gears and running at high speeds to achieve decent volumetric efficiencies (Taft, 1972). Flooding the compressor with oil provided both cooling, allowing higher pressure ratios without associated thermal stress, and the elimination of timing gears. Water flooding allows to avoid oil contamination of the air but required more expensive materials (corrosion-resistant) and more accurate manufacturing (Zimmern, 1984; Nikolov and Bruemmer, 2014). The first compression of a pure refrigerant in the two-phase region was experimentally investigated in a single-screw compressor around 1969 (Zimmern, 1984). The idea was, like for the water flooding of air, to have the same fluid in the liquid phase and the vapor phase (in the form of humidity for air). Moreover, oil-flooding screw compressors required to reach better manufacturing anyway, allowing low-viscosity liquid to provide sufficient sealing effect, as the refrigerant solved in the oil was reducing the viscosity of the liquid phase. The authors could achieve 70% of isentropic efficiency with a 30 kW compressor using R22 as working fluid. More recently, it has been numerically shown that the compression of wet refrigerant can achieve high isentropic efficiencies (up to 89%) and a significant discharge temperature reduction, within a twin-screw compressor (Ferreira et al., 2006b).

Liquid-flooding compression in scroll machines, like in screw machines, has many advantages, in addition to the sealing effects brought by the liquid blocking the gap between two working chambers, it also allows to get closer to an isothermal process, reducing the thermal stress on the moving parts (Bell et al., 2012a). Nevertheless, some drawbacks can also be found: the increase of the pressure losses in suction/discharge ports due to either the reduction of the speed of sound or the increase of the fluid density. Liquid-flooded scroll compressors were already being experimented before 1988, when the scroll technology was still viewed as an interesting technology with limited potential by engineers. According to Bush and Elson (1988), scroll compressors tolerance to liquid refrigerant flooding is unlimited as demonstrated by minimal scroll reaction to cold start-up and heat pump defrosting. However, this tolerance is justified by the slow compression process providing ample time for leakages, especially when a compliant design is used. In Sakuda et al. (2001), an experimental investigation

⋆The project source of the results presented in this paper has received funding from the European Union's Horizon 2020 research and innovation programme under grant agreement N° 851541.

n.leclercq@uliege.be (N. Leclercq);
benedikt.bederna@tu-dresden.de (B.G. Bederna);
vincent.lemort@uliege.be (V. Lemort)

Nomenclature

OCR	Oil Circulation Ratio [-]
MAE	Mean Absolute Error [-]
MAD	Mean Absolute Difference [-]
MRE	Mean Relative Error [-]
CV	Cross-Validation
M	influenced variable [-]
m	influencing variable [-]
h	enthalpy [J kg^{-1}]
$\dot{Q}$	heat transfer [W]
$\dot{W}$	mechanical power [W]
Q	vapor quality [-]
x	liquid mass fraction [-]
z	global mass fraction [-]
T	Temperature [K]
P	Pressure [Pa]
AU	heat transfer coefficient [W/K]

Sub/super-scripts

su	supply
ex	exhaust
mix	mixing
o	oil
r	refrigerant
amb	ambient
v	vapor
l	liquid
σ	at saturation
$\star$	corrected
is	isentropic
v	volumetric
f	friction
cp	compressor
tot	total

Greek symbols

μ	uncertainty [-]
ε	efficiency [-]
ρ	density [kg/m^3]
ω	rotational speed [rad/s]
τ	torque [Nm]

of oil-flooded compressor for performance improvement is performed. The results show that the cycle efficiency always decreases with increasing oil rates. Hiwata et al. (2002) investigated oil-injection into a CO_2 scroll compressor, where the axial compliance had been reinforced by controlling the thrust force of the orbiting scroll. The results showed the existence of an optimal oil flooding rate ranging between 6 and 15% in mass. More recently, (Bell et al., 2012b) investigated the performance of an oil-flooded off-the-shelf open-drive scroll compressor with large amounts of oil that showed no significant decrease in performance.

Feeding a scroll compressor with two-phase refrigerant could, as for the screw machine, allow to get rid of the oil while keeping a sealing effect from the liquid phase and allow a reduction of the discharge temperature. Moreover, the use of two-phase compression could bring some innovations to conventional thermal systems, as no superheat is met before and after the compressor. In Vorster and Meyer (2000), the investigation of two-phase compression in a heat pump is conducted numerically using wet fluids and non-azeotropic mixtures with high vapor qualities, and the results show a better COP when no superheat occurs in the cycle. The same results has been found, using experimental data,

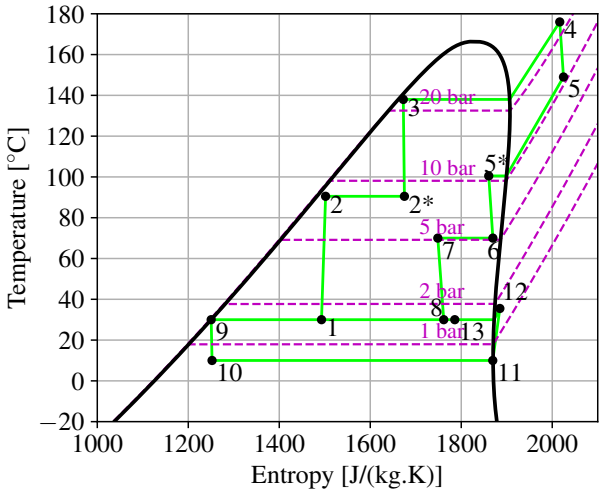

Figure 1: REGEN-BY-2 cycle Temperature-Entropy diagram.

in Leclercq et al. (2023), where saturated vapor at the compressor inlet resulted in the best trade-off between exergy destruction rate in the compressor and in the condenser. Compression-resorption heat pumps can also benefit from two-phase compression, in particular, from the compression of non-azeotropic refrigerant mixtures. In this particular technology, higher performance can be achieved using wet compression rather than a liquid-vapor separator followed by a dry compressor and a liquid pump (Ferreira et al., 2002). In Ferreira et al. (2006a), an experimental investigation is carried out on an ammonia-water compression-resorption heat pump using an oil-free twin-screw compressor. Liquid-injection ports design and positions are discussed and a maximum compressor isentropic efficiency of 50% could be obtained with the liquid-injection occurring in the compression start phase. A more recent study from the same authors (Gudjonsdottir et al., 2019) showed that an isentropic efficiency above 70% could be achieved for a particular design, with inlet vapor qualities ranging from 0.5 to 0.7, without under and over-compression. Finally, the innovative cycle currently being developed in the REGEN-BY-2 European project (Horizon 2020) is also making use of two-phase refrigerant to operate (Briola et al., 2021). The Temperature-Entropy diagram of this cycle can be found in Figure 1. It is in the frame of this European project that the test bench presented in this article has been developed. The objetive is the characterization of the two-phase compressors, part of the REGEN-BY-TWO cycle. A retrofitted compressor was first tested to validate a deterministic model, then, a lab-scale prototype, intended to be used in the final plan, has also been characterized. Nevertheless, the test bench design allows the testing of numerous volumetric machines with two-phase (oil-) refrigerant flows, although the operating ranges could be limited.

In this article, the test bench dedicated to the two-phase scroll compressors testing is first described. Its configuration as well as the actuators used to control the compressor operating conditions are presented. The sensors employed

in the test bench are discussed and their operating ranges and uncertainty given. Moreover, details are given about the test bench materials and equipments disposition. Second, the post-processing methodology, to figure out the vapor quality as well as the compressor performance indicators, is introduced. Furthermore, some calibration techniques required to achieve good accuracy in the results are developed. The use of a gaussian prediction tool allows interpolation and extrapolation of the results, with some limitations. Finally, the compressor performance results of three testing campaigns are discussed and conclusions are drawn.

2. Test bench description

2.1. Test bench conception

The layout of the test bench is inspired from a heat pump and can be found in Figure 3. This test bench is dedicated to characterize the compressor performance, namely, to measure its volumetric and isentropic efficiencies over a wide range of operating conditions. The compressor is an open-drive automotive scroll compressor, the model is the TGVE08 from Sanden. It has a displacement volume of 86 cm^3 and a built-in volume ratio of 2.3. This compressor operates without a compliance mechanism, keeping constant radial and axial gaps. The orbiting movement of the orbiting scroll is ensured by a crank pin inserted into the orbiting scroll bearing. Metallic balls are trapped between the orbiting scroll and a cage connected to the casing, allowing relative movement between the scroll without rotation, as depicted in Appendix A. This orbiting mechanism has been patented by Sanden (Ni, 2008). Those metallic balls also allow to keep the axial and radial gaps constant, even when an overturning moment is generated by the chambers pressure. A reed valve is placed on the discharge port, avoiding backflow inside the discharge chamber. The compressor is powered with an electric motor and a torquemeter is used to measure its power consumption. Moreover, lubrication is ensured by an independent oil loop allowing to regulate the oil circulation ratio (OCR) using the valve V3. To separate the oil from the refrigerant, the two-phase oil-refrigerant mixture is heated up by a resistor at the outlet of the compressor to vaporize the refrigerant, the oil is then recovered by an oil separator. The oil is then cooled and redirected at the inlet line of the compressor, called "mixing line". After the oil separator, a part of the vapor is redirected directly towards the mixing line while the remaining part is condensed and subcooled. By varying the opening of the three controlled discharge valves (V1, V2, V3), a wide range of conditions can be met, allowing to test different pressure ratios, inlet pressures, inlet vapor qualities and OCR. Furthermore, the compressor speed can also be controlled using a variable-frequency drive. A pulley ratio of 1.7 between the motor and the compressor allows to run the compressor with a speed up to 5000 RPM.

The test bench 3D representation can be found in Figure 2, it uses the same legend as in Figure 3. A picture of the test bench is also available in Appendix B. As can be observed, the compressor has been placed vertically to avoid liquid accumulation in the discharge chamber. The liquid, present in the discharge chamber, will therefore naturally flow toward the discharge port reed valve and be ejected from the compressor. In the case of a liquid accumulation leading to a pure-liquid compression, a torque limiter has been placed on the shaft coupling, disengaging when excessive torque is encountered. The latter mechanism allows to protect both the compressor and the torquemeter. Moreover, the heating resistor has a 2.4 meters length, it has been designed to provide a surface power exchange of 1.9 W/cm^2 to avoid oil degradation due to too high temperatures, its maximum power rating being 30 kW. As can be observed, it has been placed diagonally, to facilitate the entrainment of the oil with the gravity, as the speed of the refrigerant is not high enough within this cross-section area. The refrigerant used is the HCFO R1233zd(E), and a total of 20 kg has been filled in the test bench. The lubricating oil is either the Emkarate RL32 MAF or a mixture between the RL32 and a POE40 from Petronas depending on the test campaign. Regarding sealing joins, the compatibility between the refrigerant and plastic/elastomers has been investigated, as bad experience from the past already occured with this kind of fluid. According to Honeywell (2018), Viton is suitable for use as its volume only increases between the flanges, with a 8.6% volume expansion observed after two weeks of immersion. Nevertheless, it appears that sealing join degradation has been observed anyway, requiring the flanges to be regularly tightened to prevent leakages.

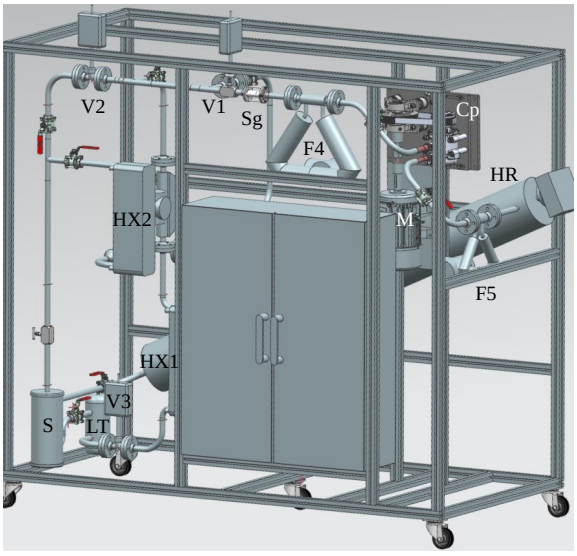

Figure 2: Test bench 3D representation.

2.2. Measurement techniques/instrumentation equipments

The precise characterization of the compressor's performance requires a complete set of intrumentation equipments. Firstly, numerous temperature/pressure measurements are taken, mainly to check the energy balances all over the test bench. Furthermore, the mass flow rates of each line

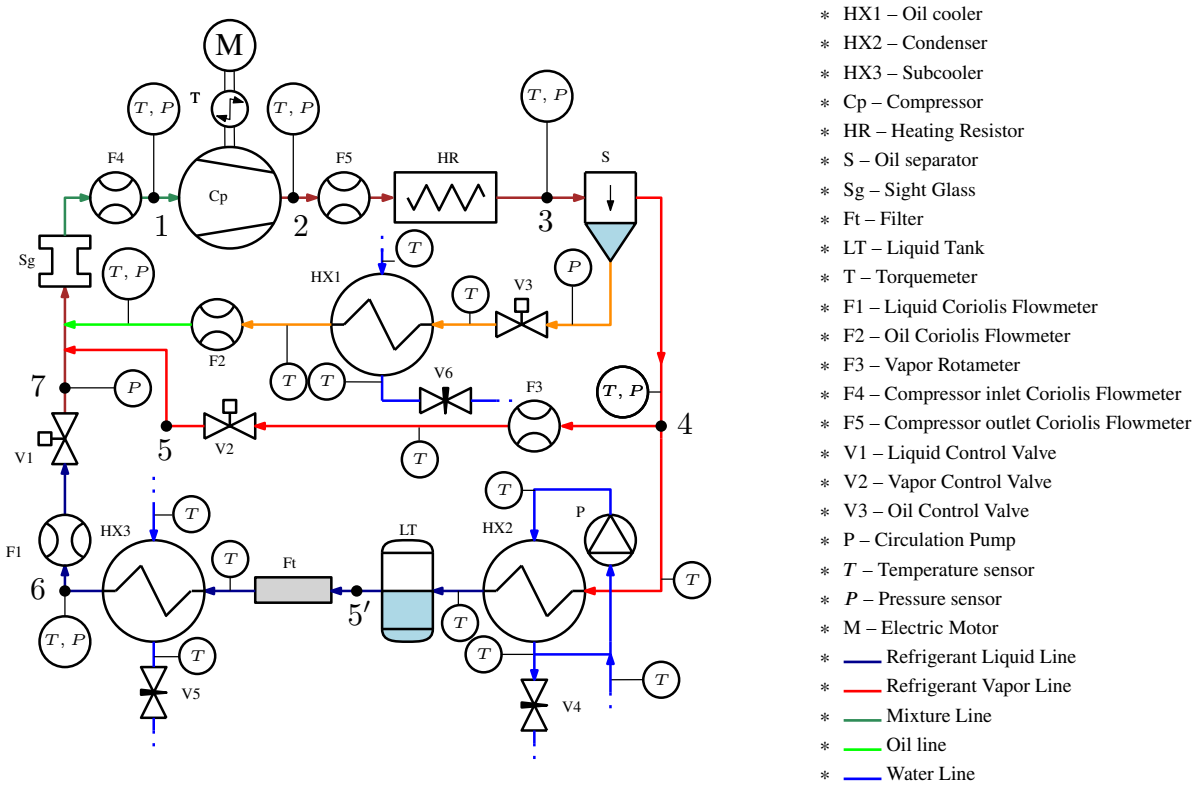

Figure 3: Test bench layout.

(refrigerant vapor, refrigerant liquid and oil) are measured, using Coriolis flowmeters for the oil and the liquid lines and a rotameter for the vapor line. The cooling water mass flow rates are also measured using electromagnetic flowmeters to check the energy balances of the three heat exchangers. A cylindrical sight glass has been placed in the mixing line in order to see the flow, particularly useful at the test bench start-up, to ensure the operating conditions are optimal before increasing the speed of the compressor (limited presence of liquid). Nevertheless, this sight glass does not allow any image processing to figure out further data regarding the flow. Regarding the inlet vapor quality, it is figured out using an energy balance on the mixing line (line from which the mixing is done, upstream of the compressor), the details will be shown in the subsequent section. The key issue faced in the design of the test bench is the evaluation of the vapor quality with a decent accuracy. No sensor allows measuring the vapor quality directly as most of the time, the sensors used in the literature are measuring parameters that can be correlated with vapor quality. A review of the vapor quality assessment has been conducted, showing that most of the sensors are neither reliable nor mature. The two main types that are easily applicable are the capacitive and the Coriolis, allowing measurement of the void fraction. However, this void fraction can not always be easily linked with the vapor quality of the flow, as non-unity slip ratio can appear. Two Coriolis flowmeters from the Emerson's Elite series have been installed on the test bench, before and after the compressor, with the purpose of measuring the density at the compressor inlet/outlet. It however appeared that they only deliver good accuracy when high (> 0.95) or low vapor (< 0.1) quality are tested. These Coriolis flowmeters are therefore used to calibrate the vapor rotameter with superheated conditions, in order to match the total mass flow rate obtained with the mass flow rates of each line measured individually ($\dot{m}_{F1} + \dot{m}_{F2} + \dot{m}_{F3} = \dot{m}_{F4} = \dot{m}_{F5}$, in Figure 3). As already mentioned, a torquemeter is used to measure the torque on the motor shaft, moreover, it also provides speed measurement eventually allowing to obtain the mechanical power developed by the motor. This power, however, is different from the power provided to the compressor, as the power is transmitted via a pulley-belt mechanism inducing power losses.

Eventually, the models of the sensors employed on the test bench, their operating range as well as their uncertainties can be found in Table 1. The measurements uncertainties propagation is going to be studied through the post-processing methodoly to check its impact on the determined performance indicators. The absolute uncertainty μ_M of a calculated variable M is calculated by:

$$\mu_M = \sqrt{\sum_i \left(\frac{\partial M}{\partial m_i} \mu_i \right)^2} \tag{1}$$

where μ_i are the uncertainties of each measured/used values m_i used to compute M (Bell et al. (2012b)).

Table 1
Sensors used, range and uncertainties.

Sensor	Equipment	Range	Uncertainty
Pressure sensors	Keller PAA21Y	0 - 10 [bara]	0.05 [bar]
Temperature sensors	T-thermocouple	-185 - 300 [°C]	0.5 [K]
Torquemeter	ETH DRV-II-20Nm	0 - 20 [Nm]	0.02 [Nm]
Compressor inlet Coriolis Flowmeter	Emerson Elite CMF100M	15 - 333 [g/s]	0.25%
		0 - 5000 [kg/m^3]	0.5 [kg/m^3]
Compressor outlet Coriolis Flowmeter	Emerson Elite CMF050M	3 - 333 [g/s]	0.1%
		0 - 5000 [kg/m^3]	0.5 [kg/m^3]
Liquid Coriolis Flowmeter	Emerson R025S	2 - 180 [g/s]	0.5%
Oil Coriolis Flowmeter	Bronkhorst Cori-Flow M55	1 - 33 [g/s]	0.2%
Vapor Rotameter	Krohne H250 M40	6 - 60 [g/s]	0.9 [g/s]

3. Data post-processing

3.1. Tests campaigns

The objective of the test campaigns is to record numerous steady-state operating points, varying the compressor speed, inlet pressure, pressure ratio, OCR as well as the inlet vapor quality, to calculate the isentropic and volumetric efficiencies of the compressor, also called performance indicators. Three test campaigns have been conducted on the test bench. First, a test campaign using the oil Emkarate RL32 MAF as a lubricant allowed to test 142 operating points, with a compressor speed ranging from 1000 RPM to 5000 RPM, and a vapor quality from 0.35 to highly superheated conditions, as represented in Figure 4. A second test campaign, where a partial replacement of the oil has been performed, allowed to record 71 points, only at the speed of 2000 RPM. An oil mixture composed of 39% of RL32 and 61% of a POE40 from Petronas was therefore used during this campaign. The two tested oils have dynamic viscosities of 32 mPas and 37 mPas at 40°C, for the pure oil and the oil mixture, respectively. A third test campaign allowed to test the compressor without oil at two speeds (2000 and 3000 RPM), for a total of 72 points, including 23 points with superheated inlet conditions. The x-axis in Figure 4 represents the difference between the measured temperature and the refrigerant saturation temperature at the measured pressure, called apparent vapor superheat. As can be observed, even when two-phase conditions (vapor quality below 1) are met, a superheat is measured, result of the zeotropic behavior brought by the oil. Only a few points meet this behavior when no oil is used, which could be the result of thermal non-equilibrium between the liquid and the vapor phases, inducing error in the temperature measurement. The inlet vapor quality represented on the plot is the ratio between the vapor mass flow rate and the total mass flow rate at the compressor inlet.

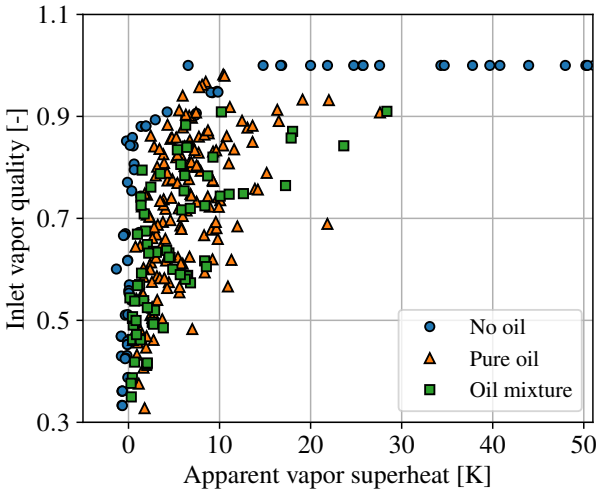

Figure 4: Datapoints collected from the three experimental campaigns.

3.2. Vapor quality determination methodology

A vapor quality determination methodology has already been presented by the authors in Leclercq et al. (2023), with some of the experimental data presented in this article. Three assumptions were used to apply an energy balance on the mixing line, allowing the determination of the unknown inlet quality. This article improves the assumptions as follows:

1. In the previous method, it was assumed that no refrigerant is flowing in the oil line after the oil separator, as a minimum apparent superheat is ensured at the outlet of the heating resistor. Nevertheless, oil-refrigerant solubility experimental data supports that, even with a high apparent superheat, refrigerant fraction in the liquid phase is non-negligible. Therefore, oil-refrigerant data measurements were used to estimate the liquid phase composition after phases separation. Regarding the oil fraction in the vapor phase after separation, it is neglected as the saturation pressure of the oil is extremely low compared with the refrigerant (Scialdone et al., 1996).
2. Thermal equilibrium was assumed before the compressor where the temperature of the mixture is measured. This assumes that the liquid phase and the vapor phase have the same temperature. However, depending on the operating point measured, it may be possible that this equilibrium is not reached, thereby inducing errors on the

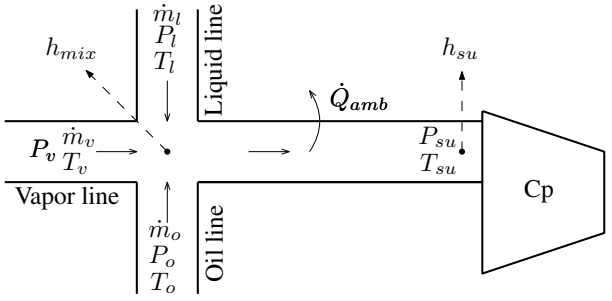

Figure 5: Representation of the mixing line.

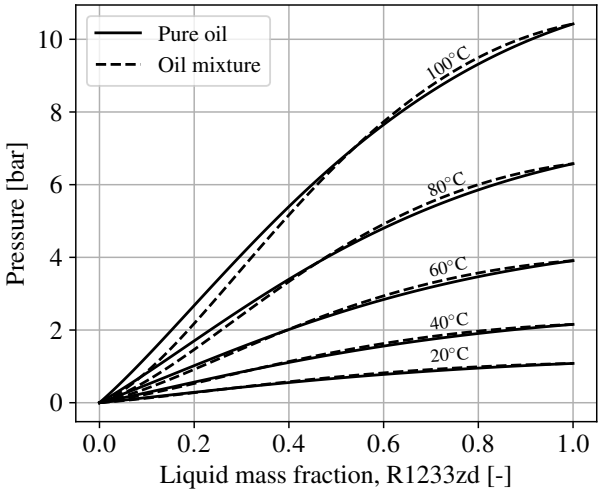

Figure 6: P×T diagram predicted by Cavestri's equation for both oil-refrigerant mixtures.

inlet temperature measurement. Thus, a new methodology is proposed to figure out the vapor quality. This new methodology does not assume thermal equilibrium at the inlet of the compressor as it does not use the inlet temperature measurement. It is also based on oil-refrigerant solubility data and therefore assumes a mixture equilibrium (solubility equilibirum reached). A comparison of the two proposed methodologies is presented later in the article.

3. No thermal losses were taken into account in the mixing line, so that the energy balance from the mixing point to the compressor inlet could be respected without heat losses. This assumption was deemed reasonable as the pipe is well insulated, moreover, for some points, the mixture reaches temperature close to the ambiance temperature (≈ 20°C) in the low-pressure side (R1233zd(E) has a boiling point of 19°C). Improvement on this side has been brought using the 23 superheated points without oil, enabling the estimation of the heat losses through temperature and pressure measurements only.

A representation of the mixing line, on which an energy balance is applied, can be found in Figure 5. The applied energy balance is written as follows:

$$h_{su} = h_{mix} - \frac{\dot{Q}_{amb}}{\dot{m}_{tot}} \tag{2}$$

The enthalpies are calculated using the ideal mixture assumption between the oil and the refrigerant (neglected mixing term) (Youbi-Idrissi and Bonjour, 2008). As underlined in the assumption 1, the fraction of refrigerant solved in the oil ($x_{r,o}$) is taken into account in the calculation. This gives:

$$\begin{aligned} h_{mix} = {} & Q_{mix} h_{r,v}(P_v, T_v) + z_o x_{r,o} h_{r,l}(T_o, P_o) \\ & + z_o(1 - x_{r,o}) h_o(T_o) + (1 - Q_{mix} - z_o) h_{r,l}(P_l, T_l) \end{aligned} \tag{3}$$

$$\begin{aligned} h_{su} = {} & Q_{su} h_{r,v}(P_{su}, T_{su}) + z_o x_{r,o} h^{\sigma}_{r,l}(T_{su}) \\ & + z_o(1 - x_{r,o}) h_o(T_o) + (1 - Q_{su} - z_o) h^{\sigma}_{r,l}(T_{su}) \end{aligned} \tag{4}$$

where the conditions (temperatures, pressures and mass flow rates) coming from the three main lines (refrigerant vapor (r, v), oil (o) and refrigerant liquid (r, l)) and the supply (su) of the compressor are known. Moreover, the mixing quality is given by $Q_{mix} = \frac{\dot{m}_v}{\dot{m}_{tot}}$, the OCR is $z_o = \frac{\dot{m}_o}{\dot{m}_{tot}}$ and the total mass flow rate $\dot{m}_{tot} = \dot{m}_v + \dot{m}_l + \dot{m}_o$ is also coming from the measurements. The compressor inlet enthalpy uses $h^{\sigma}_{r,l}$, the saturated liquid (σ) enthalpy of the refrigerant. The refrigerant properties are computed using CoolProp and the pure oil properties as well as the oil-refrigerant solubility data are retrieved from Leclercq et al. (2024), where the Cavestri equation is fitted using experimental data to estimate the vapor pressure of the first oil-refrigerant mixture. Experimental data have also been obtained for the second oil-refrigerant mixture. The Cavestri equation and the corresponding fitted parameters can be found in Appendix C. Moreover, a representation of the solubility curves for both oil-refrigerant mixtures can be found in Figure 6.

Therefore the liquid refrigerant mass fraction $x_{r,o}$ is a function of the temperature and the pressure measured right before the oil separator. The corrected oil circulation calculated due to the presence of liquid refrigerant in the oil can is defined as:

$$z^{\star}_o = z_o(1 - x_{r,o}) \tag{5}$$

The ambient losses in Equation 2 are expressed using the following equation:

$$\dot{Q}_{amb} = AU_{amb}(T_{su} - T_{amb}) \tag{6}$$

Where AU_{amb} is determined, as explained in assumption 3, using 23 inlet superheated points without oil circulation. These superheated points allow to calculate h_{mix} and h_{su} from measurements only. The methodology to determine AU_{amb} is therefore written as:

$$AU_{amb} = \arg\min \sum_k \left[h^k_{mix} - h^k_{su} + \frac{AU_{amb}}{\dot{m}^k_{tot}} \left(T^k_{su} - T^k_{amb} \right) \right] = 3.05 \text{ [W/K]} \tag{7}$$

Where k is the index used to loop over the superheated points.

The previous methodology (Leclercq et al., 2023) used to determine the vapor qualities simply applies the energy balance written in Equation 2, as all pressures, temperatures and mass flow rates of each lines are measured. Therefore, when combining Equations 3, 4 and 2, the only remaining unknown is the inlet vapor quality Q_{su}. This methodology assumes a thermal equilibrium between the two phases at the compressor inlet, as it uses the uniform measured temperature T_{su}. In the new methodology, the energy balance in Equation 2 is also applied. However, the compressor inlet temperature T_{su} is not going to be taken from the measurements anymore, and will become an unknown of the system. This allows getting rid of the thermal equilibrium assumption. Nevertheless, a new equation must be added, which is the solubility equation applied to the two-phase oil-refrigerant mixture. For both oils employed, the Cavestri equation is again used to determine the refrigerant liquid fraction at the compressor supply $x_{r,su}$, as a function of the inlet temperature and pressure. Moreover, applying the lever rule allows to link the inlet vapor quality to the inlet temperature, pressure and OCR. This equation is written as:

$$Q_{su} \cdot \left[1 - x_{r,su}(P_{su}, T_{su}) \right] = 1 - z^\star_o - x_{r,su}(P_{su}, T_{su}) \tag{8}$$

The unkowns of the new system of equations are thereby Q_{su} and T_{su}. The limitation of this new methodology lies in its reliance on a good mixing between the oil and the refrigerant, so that the solubility equation can be applied. The measured temperature T_{su} is going to be replaced by the newly calculated temperature in the following developments.

The relative error between the vapor quality calculations from the previous and the new methodologies are represented as a function of the apparent superheat in Figures 7 and 8, without and with OCR correction, respectively. The uncertainty propagation from the vapor quality determination is also included in the relative error calculation, and represented on both figures. The idea behind the representation of the uncertainty is to check if the 0-error axis is crossed by the red line (uncertainty), in which case the error propagation could explain the deviation between the two methodologies.

An important observation derived from the two figures is the clear improvement of the results when the refrigerant solved in the oil line is taken into account. The correction of the OCR allows the mean relative error (MRE) to decrease from 5.18% to 1.67%, which is non-negligible. Eventually, the comparison between the two methods with OCR correction still presents some points where the uncertainty

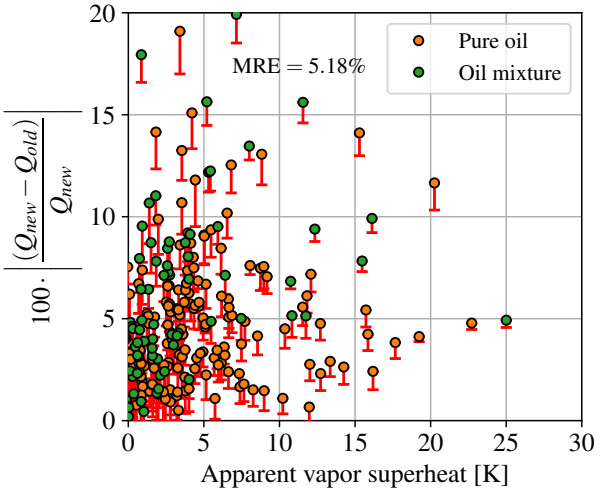

Figure 7: Relative error between the vapor qualities coming from previous and new methodologies without correction of the OCR.

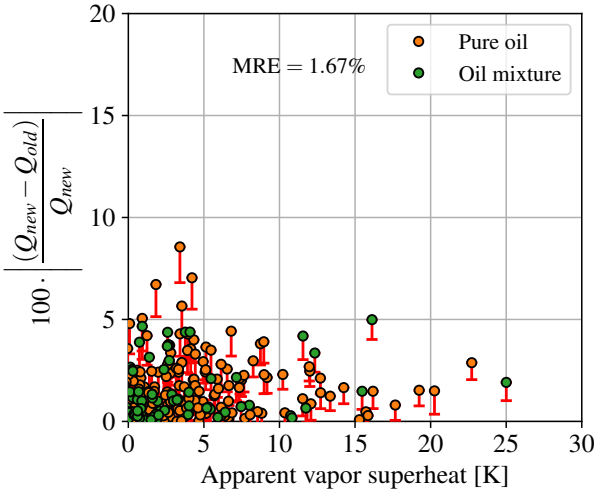

Figure 8: Relative error between the vapor qualities coming from previous and new methodologies with correction of the OCR.

propagation does not justify the difference. The difference between those specific points comes either from the thermal or the mixing non-equilibrium. Nevertheless, the relative error always remains below 10%, providing a good approximation of the vapor quality from both methodologies. The difference between the newly calculated inlet temperature and the measured temperature is displayed in Figures 9 x-axis, while the difference in vapor qualities, volumetric and isentropic efficiencies is plotted on the y-axis. As can be seen, the mean absolute difference (MAD) between the two methologies is low, especially for the performance indicators where the MAD stand below 1%, which supports the hypothesis that both methodologies are valid.

3.3. Volumetric efficiency

The volumetric efficiency of the compressor compares its measured mass flow rate with its theoretical mass flow

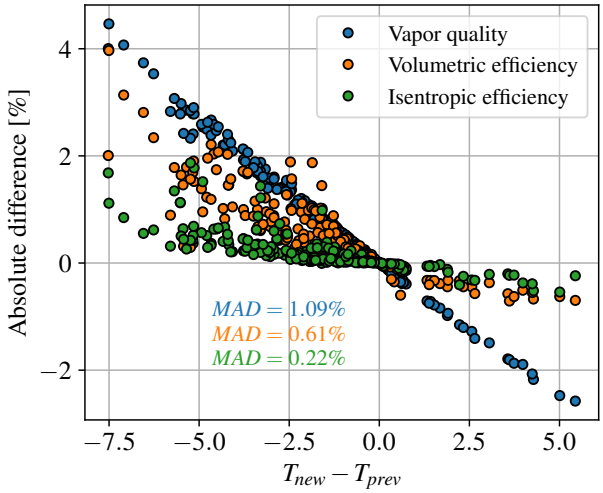

Figure 9: Absolute difference in vapor quality, volumetric and isentropic efficiency and a function of the inlet temperature difference between the new and the previous methodologies, for the whole dataset.

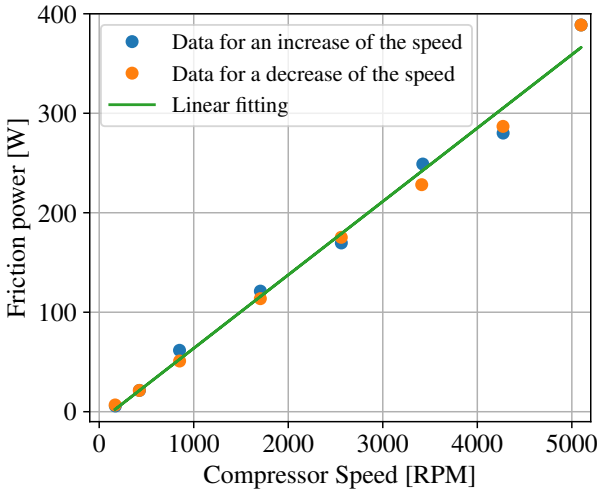

Figure 10: Power dissipated by the pulley-belt mechanism without load at different compressor speeds.

rate, by multiplying the inlet density (ρ_{su}) by the volumetric flow rate, computed by multiplying the speed the compressor (N_{cp}) and its displacement volume (V_{disp}). It can be computed using the following equation:

$$\varepsilon_v = \frac{\dot{m}_{tot}}{N_{cp} V_{disp} \rho_{su}} \tag{9}$$

Considering an ideal mixture, the inlet density can be calculated by:

$$\begin{aligned} \rho_{su}^{-1} = {} & Q_{su} \rho_{r,v}^{-1}(P_{su}, T_{su}) + z_o^\star \rho_o^{-1}(T_{su}) \\ & + (1 - Q_{su} - z_o^\star)\, {\rho_{r,l}^\sigma}^{-1}(T_{su}) \end{aligned} \tag{10}$$

3.4. Isentropic efficiency

The isentropic efficiency compares the ideal power consumption of the compressor with its real power consumption and can be obtained from:

$$\varepsilon_{is} = \frac{\dot{m}_{tot}(h_{ex,is} - h_{su})}{\dot{W}_{shaft,cp}} \tag{11}$$

with $h_{ex,is}$ the outlet enthalpy following an isentropic (adiabatic and reversible) compression and $\dot{W}_{shaft,cp}$, the power received at the compressor shaft, defined as:

$$\dot{W}_{shaft,cp} = \omega_{mot} \cdot \tau_{shaft,mot} - \dot{W}_{f,belt} \tag{12}$$

with $\dot{W}_{f,belt}$ the power loss from the pulley-belt mechanism, that could be directly measured disengaging the clutch of the compressor while measuring the torque developed when running the motor at different speeds as represented in Figure 10.

The definition of the isentropic compression outlet enthalpy of a two-phase oil-refrigerant mixture is inspired from the definiton of Ramaraj et al. (2014), where the entropy exchange between the oil and the refrigerant is taken into account. However, the authors did not consider the part of refrigerant solved in the oil, as their inlet superheats were high enough to neglect it. A new definition is therefore proposed, for which two unknowns have to be defined:

- The isentropic temperature T_{is}
- The isentropic vapor quality Q_{is}

Those two unknows will allow to compute the isentropic enthalpy as follows:

$$\begin{aligned} h_{is} = {} & Q_{is} h_{r,v}(P_{ex}, T_{is}) + z_o^\star h_o(T_{is}) \\ & + (1 - Q_{is} - z_o^\star) h_{r,l}^\sigma(T_{is}) \end{aligned} \tag{13}$$

Two equations are necessary to solve the system with the two previously defined unknowns: the conservation of entropy along the compression and the oil-refrigerant solubility equation. The oil-refrigerant solubility equation will be derived similarly to the methodology used to determine the vapor quality. The system to solve is therefore the following, with $s_{su} = s_{ex,is}$:

$$\begin{cases} s_{su} = Q_{su} s_{r,v}(P_{su}, T_{su}) + z_o^\star s_o(T_{su}) \\ \qquad +(1 - Q_{su} - z_o^\star) s_{r,l}^\sigma(T_{su}) \\ s_{ex,is} = Q_{is} s_{r,v}(P_{ex}, T_{is}) + z_o^\star s_o(T_{is}) \\ \qquad +(1 - Q_{is} - z_o^\star) s_{r,l}^\sigma(T_{is}) \\ Q_{is} \left[1 - x_{r,is}(P_{ex}, T_{is})\right] = 1 - z_o^\star - x_{r,is}(P_{ex}, T_{is}) \end{cases} \tag{14}$$

The isentropic work determination process is illustrated in Figure 11. The crossing point between the two temperature lines defines the isentropic quality. It thus finds the temperature and vapor qualities allowing to respect the conservation of entropy and the solubility equation of the mixture. The obtained vapor quality then allows to get the isentropic work (illustrated by the green arrow).

3.5. Interpolation tool

In order to get rid of the dependency of the inlet quality Q_{su} on $z_o^\star$ (the higher the OCR the lower the vapor quality),

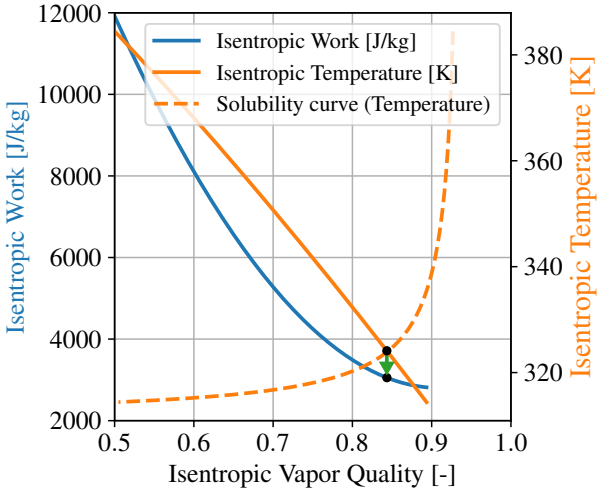

Figure 11: Illustration of the isentropic work calculation.

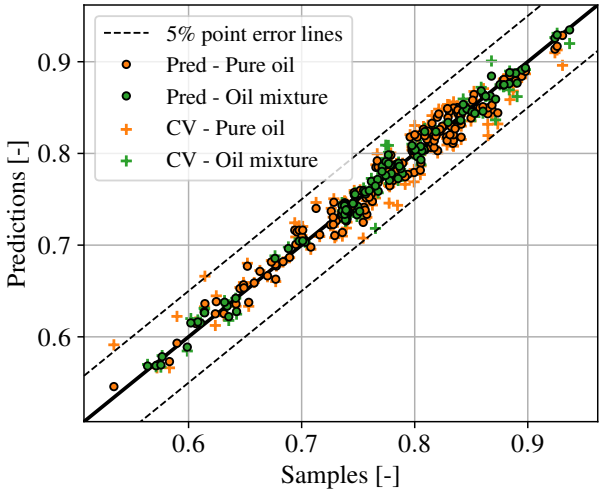

Figure 12: Datasets versus predictions (Pred) and cross-validation (CV) for the volumetric efficiency.

all results will be plotted as a function of a refrigerant-only vapor quality (varying between 0 and 1), defined as: $Q_{r,su} = Q_{su}/(1 - z_o^\star)$. This vapor quality could in theory never be equal to one, as it would mean a high enough apparent superheat allowing to have 0% refrigerant solved in the oil. The results coming from this refrigerant-only vapor quality will still have some slight dependency on the OCR, as the higher the OCR, the higher the liquid mass fraction (oil comprised) for the same refrigerant-only vapor mass fraction.

In total, 5 variables can influence the compressor performances:

1. The compressor inlet pressure P_{su}
2. The oil circulation ratio z_o
3. The compressor speed N_{cp}
4. The inlet vapor quality $Q_{r,su}$
5. The compression ratio r_p

All those variables have varying degrees of impact on both isentropic and volumetric efficiencies of the compressor. However, it is impossible to get a high number of experimentally tested values for each variables for two reasons. First, the test bench limitations do not allow to test any conditions, for instance, the mass flow rate varies from 4 g/s (high quality with a low speed) to 90 g/s (low quality with a high speed), meaning that the pressure losses in the test bench will only allow to test high compression ratios at high speeds. Then, too many operating points are needed to test each variable with many values, for instance, if 4 fixed values were to be tested for each variable, the total number of operating points would be $4^5 = 1024$, which is impractical.

Therefore, instead of targeting all possible points, a useful predictive tool has been used to interpolate points that were not recorded. The tool is called GPExp (Quoilin and Schrouff, 2016) and is a machine learning tool using Gaussian processes to predict data in the 5 dimensions given a set of points. It is able to get rid of the outliers and to perform a cross-validation (CV) with the dataset used, to prevent overfitting/underfitting. This method is applied for every point and if the total error is below a fixed tolerance, the dataset is accepted. If too much error is resulting from the cross-validation, it means that some data are missing to get accurate predictions. This tool is very accurate when points need to be interpolated, but lose its accuracy when extrapolation is performed.

In total, 184 points have been validated by GPExp for the first tests campaign (pure oil), while 106 points have been validated for the second (oil mixture, one tested speed). Moreover, the two-phase points without oil have been included in both tests campaigns. The data coming from the third tests campaign with superheated conditions are only used for sensor calibration. The fitting error as well as the cross-validation error on the volumetric and isentropic efficiency can respectively be seen in Figure 12 and Figure 13. The mean absolute errors (MAE) of the two performance indicators for both sets of points can be found in Table 3. On average, the accuracy of the interpolation (based on the cross-validation) can be trusted within a 3% point range for the volumetric efficiency and within a 2.5% range for the isentropic efficiency. It is essential to emphasize that those MAE do not take into account the mean uncertainty propagation on both volumetric and isentropic efficiency, which are equal to 4.4% and 3.7%, respectively. The variables having the most influence on the isentropic efficiency have been identified as being the inlet vapor quality and the pressure ratio. Thereby, 2D color maps have been generated to show the evolution of the isentropic and volumetric efficiencies with these operating variables for the two tested oils.

4. Results and discussion

4.1. Reference case

First, references plots of both the isentropic and volumetric efficiencies are analyzed (Figure 14 and Figure 15). Those reference plots will be used as a basis to the following

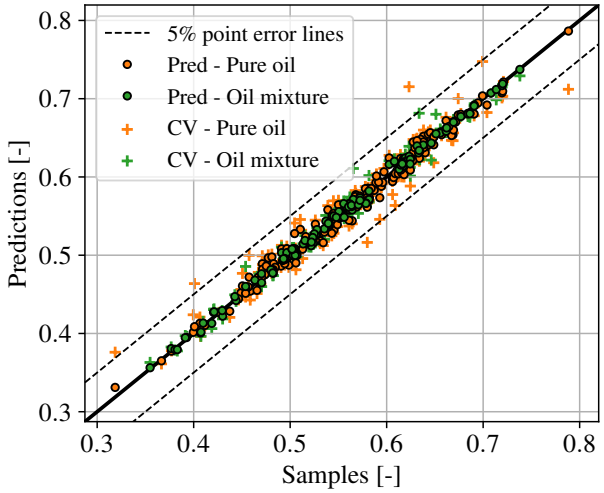

Figure 13: Datasets versus predictions (Pred) and cross-validation (CV) for the isentropic efficiency.

Table 2
Mean absolute error (MAE) of the prediction and the cross-validation for both datasets.

	Predictions		Cross-validation	
	ε_v	ε_{is}	ε_v	ε_{is}
Pure oil	2.40%	1.41%	3.55%	2.67%
Oil mixture	1.65%	0.99%	2.53%	2.19%

plots (Figures 16 to 21), displaying only the difference in efficiencies with regards to the reference, making the analysis easier. At this reference case, the speed of the compressor is fixed at 2000 RPM, which is the only speed tested for the oil mixture. The inlet pressure is set at the average tested pressure, i.e., at 1.5 bar. Moreover, tested points are represented on the reference plots, allowing to envision the whole datasets for the two compared testing campaigns, thereby allowing to see where extrapolation is performed, as it is less reliable than interpolation. The 2D reference maps of the isentropic and volumetric efficiencies can be found in Figure 14 and Figure 15. As can be seen, the experimental points almost cover the entire maps, meaning that extrapolation is limited.

It can clearly be seen that the isentropic efficiency is decreasing when the inlet quality decreases. Another tendency is the under-compression losses that are emphasized with low vapor qualities, this can be explained by the shift of the ideal pressure ratio towards lower value when lowering the qualities, as the inlet-outlet volume ratio diverges further from the compressor's built-in volume ratio. Therefore, when lowering the vapor quality, under-compression losses are increased and over-compression losses decreased. Moreover, the decrease in isentropic efficiency can also be justified with the decrease of the volumetric efficiency with low vapor qualities, which could be justified by the higher leakages faced by the compressor, as no compliance mechanism are used, at the reference speed of 2000 RPM.

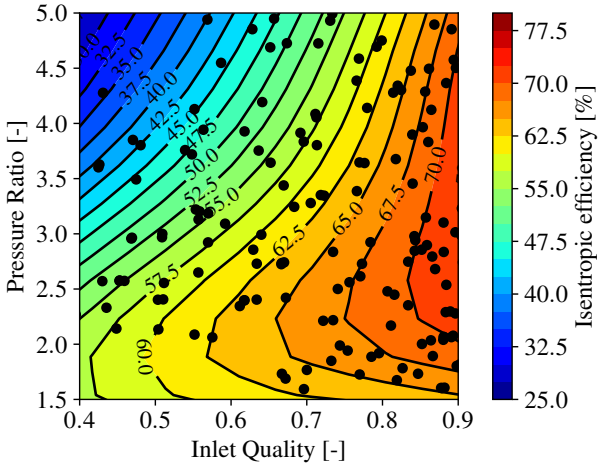

Figure 14: Evolution of the isentropic efficiency for the pure oil tested, with an inlet pressure of 1.5 bar, an OCR of 10% and a compressor speed of 2000 RPM (reference case).

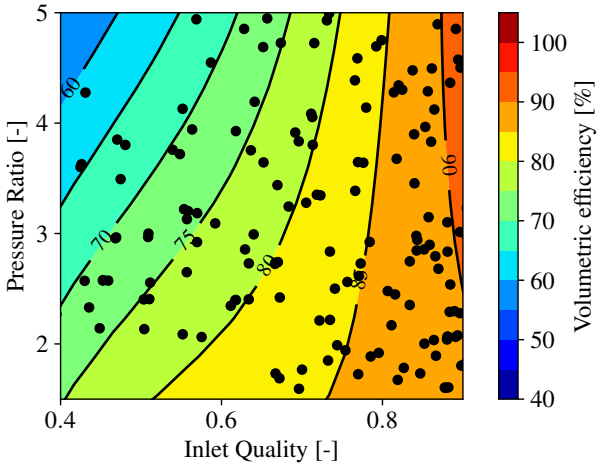

Figure 15: Evolution of the volumetric efficiency for the pure oil tested, with an inlet pressure of 1.5 bar, an OCR of 10% and a compressor speed of 2000 RPM (reference case).

This increase in leakages is attributed to the reduction in liquid-phase viscosity caused by the presence of refrigerant, combined with fixed leakage gaps.

4.2. Comparison between the two tested oils

Differences of isentropic and volumetric efficiencies compared with the reference case can be found in Figure 16 and Figure 17. Overall, the results from the two tested oils show similar tendencies, as well as similar values. Small deviations in isentropic efficiencies (around +7.5% point) appears in the zone where low qualities and high pressure ratio. Moreover, the same tendency appears in the volumetric efficiency maps. This effect could be explained by the higher viscosity and lower refrigerant solubility of the second oil, thereby increasing the liquid phase viscosity. This higher viscosity could reduce the leakages for low vapor qualities and high pressure ratio and thus increase the volumetric efficiency. Regarding the rest of the maps, the

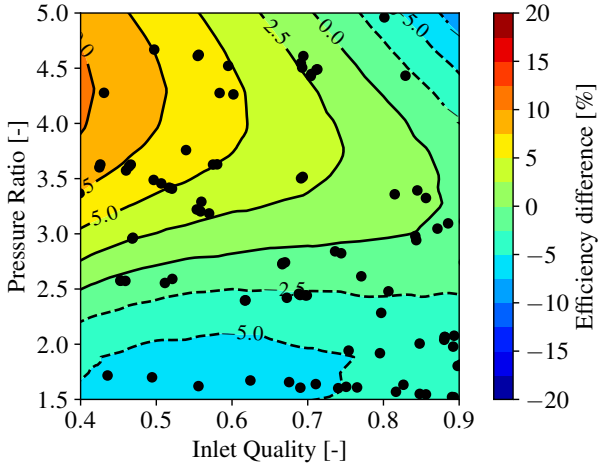

Figure 16: Difference of isentropic efficiency from the first tested oil to the second, at the same operating conditions.

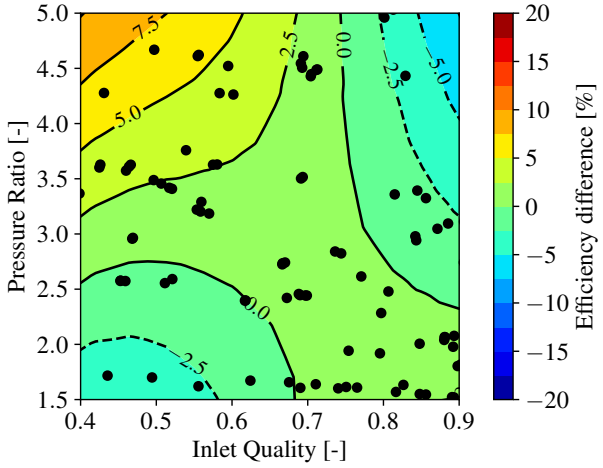

Figure 17: Difference of volumetric efficiency from the first tested oil to the second, at the same operating conditions.

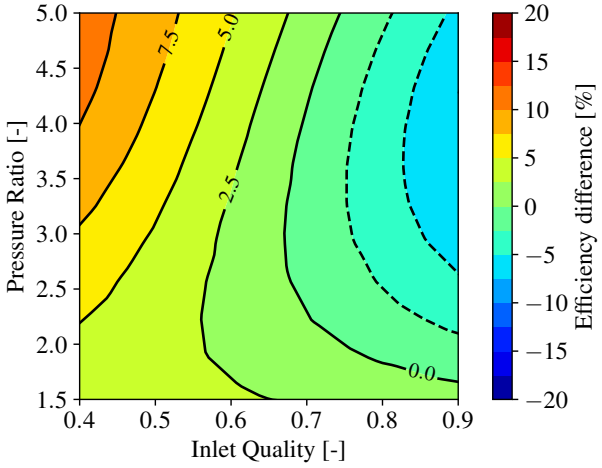

Figure 18: Difference of isentropic efficiency from the base case speed of 2000 RPM to 5000 RPM.

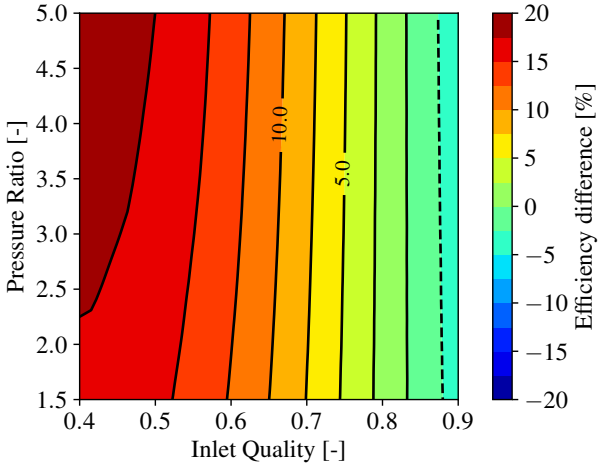

Figure 19: Difference of volumetric efficiency from the base case speed of 2000 RPM to 5000 RPM.

small deviations (< 5% point absolute) could be justified by interpolation/uncertainty errors or even lack of data for the oil mixture, which does not allow to conclude a positive/negative effect of the second oil tested. As can be justified by the distribution of experimental points on the maps, extrapolation is limited, however, less density is found with regards to the reference case, which could increase the interpolation uncertainty.

4.3. Effect of the speed

Both 2D maps of isentropic and volumetric efficiency difference with the reference case at 2000 RPM using the pure oil, where the speed has been increased to 5000 RPM, can be found in Figure 18 and Figure 19. The effect of an increase of speed at high vapor qualities seems to decrease the isentropic efficiency, which could be explained by the increase of friction losses inside the compressor, despite the increase of volumetric efficiency provided by the reduction of leakage. Nevertheless, the efficiency at low vapor qualities is enhanced, with a increase of more than 7.5% point for high compression ratios. The increase in volumetric efficiency allows to justify a reduction of leakages at low vapor qualities. Regarding the even higher increase at high compression ratios, one explanation could be the reduction of the high under-compression losses induced by the low vapor qualities, as for high speeds, the liquid could be preventing an isochoric compression when the compression chamber opens to the discharge chamber. This latter explanation requires numerical validation to be confirmed, which constitutes part of the authors' future work. An interesting results that can not be seen here regards the position of the no-difference in isentropic efficiency line (0.0 in Figure 18. This line, while increasing the speed, is being shifted more and more to the left (towards lower qualities), showing that the optimal trade-off between leakage reduction and friction generation is evolving with the speed and the vapor quality.

4.4. Effect of the OCR

Both 2D maps of isentropic and volumetric efficiency difference with the reference case at an OCR of 10% using

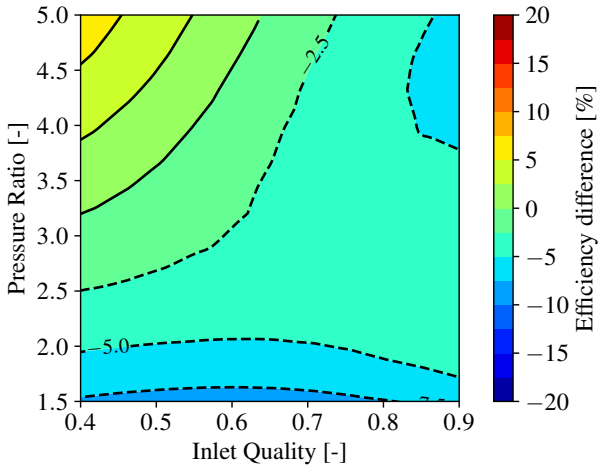

Figure 20: Difference of isentropic efficiency from the base case OCR of 10% to 5%.

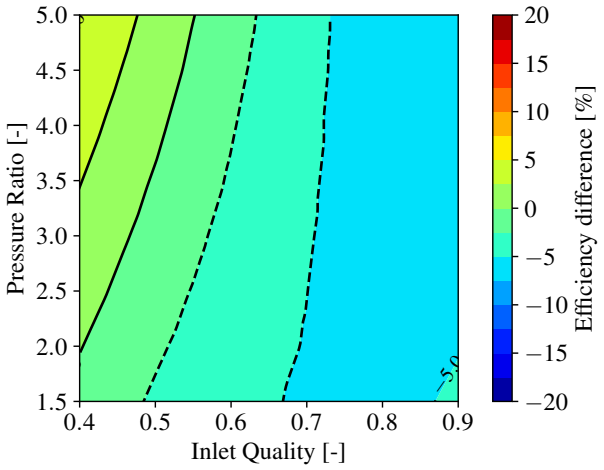

Figure 21: Difference of volumetric efficiency from the base case OCR of 10% to 5%.

the pure oil, where the OCR has been decreased to 5% can be found in Figure 20 and Figure 21. It is important to highlight the slight dependency of the refrigerant-only vapor quality, as the higher the OCR, the higher the liquid mass fraction (oil comprised) as more refrigerant is solved in the oil. Higher OCR could therefore lead to more leakages under the form of liquid, which would results in a decrease in volumetric efficiency while having a higher liquid viscosity. This effect is observed and more specifically represented in Figure 22, where, for a high pressure ratio, the OCR of 0% is leading to higher volumetric efficiencies. Overall, appart from the top-left corner of the maps (corresponding to high compression ratios in Figure 22), it seems that the higher the OCR, the better the performance, which could, once again, be explained by the higher viscosity of the liquid phase, preventing leakages. This difference is even more significant in Figure 22, where an increase of the OCR from 0 to 10% increases significantly the isentropic efficiency. Figure 22, however, shows a weird tendency at an OCR of 20% as it seems that the increases in isentropic and volumetric efficiencies when decreasing the pressure ratio does not match between each other. This could be a limitation of the interpolation algorithm actually performing extrapolation due to a lack of points at this OCR. These results can only be confirmed by applying advanced deterministic modeling techniques on the data set.

4.5. Pure refrigerant compression

Some results of the pure-refrigerant (no oil) two-phase compression can be found in Figure 23, as well as the associated uncertainties. The experimental points have been selected with some margin on the operating variables, i.e., 1±0.1 bar for the inlet pressure and 2.7±0.25 for the pressure ratio. The speed is fixed at 2000 RPM, while the OCR is zero (no oil) and the vapor quality is varying. The curves have been obtained by using GPExp and fixing the OCR to zero, which does not constitute an extrapolation as the no-oil experimental points have been included to the dataset.

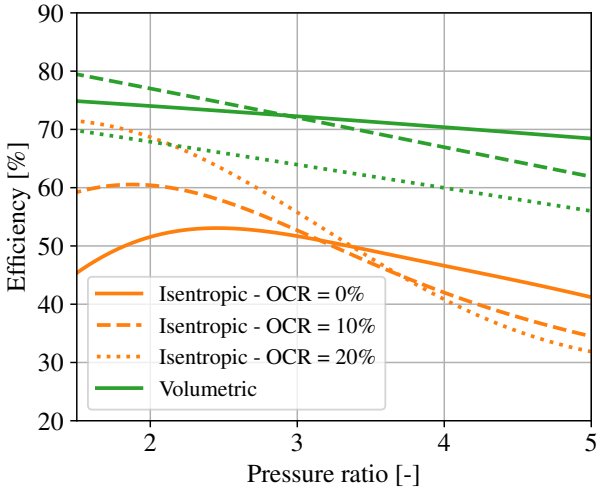

Figure 22: Isentropic and volumetric efficiencies for a varying OCR with an inlet pressure of 1.5 bar, a refrigerant vapor quality of 50% and a compressor speed of 2000 RPM.

The selected nominal pressure ratio of 2.5 is actually optimal for the given vapor quality and compressor built-in volume ratio, achieving relatively high isentropic efficiency, even at low vapor qualities. Regarding the volumetric efficiency, it is clear that a reduction in vapor quality induces an increase of the leakage, up to a point where a sealing effect is met. A superheat of 20 K has been measured for the point at a 100% vapor quality. This interpolated curve does not reach this point as points with vapor qualities of one have not been included in the algorithm because the superheat becomes a new operating variable for those points. Reformulated otherwise, different superheats can lead to different performances for a given quality of 1.

5. Conclusion

In the present article, a test bench dedicated to the investigation of two-phase compression using a retrofitted

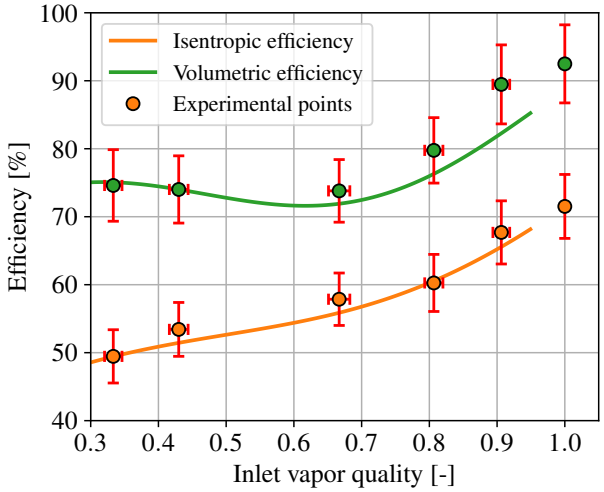

Figure 23: Isentropic and volumetric efficiencies varying with the vapor quality without oil, for a speed of 2000 RPM, an inlet pressure of 1 ± 0.1 bar and a pressure ratio of 2.7 ± 0.25.

scroll machine has been introduced and the results coming from three experimental campaign analyzed. The test bench design and architecture have been presented, as well as the sensors used to characterize efficiently the performance of the retrofitted compressor under various operating conditions. Among the experimental campaigns can be found a first campaign with as many operating conditions as possible using a given oil, and another with an oil mixture, tested at the speed of 2000 RPM. Eventually, a brief testing campaign without any oil has been conducted. The methodology to obtain the inlet vapor quality has been detailed, and the related assumptions developed. The definition of the performance indicators, i.e, isentropic and volumetric efficiencies has been shown, considering an oil-refrigerant two-phase mixture in the calculations. Eventually, a total of 253 points (with and without oil) have been used to generate 2D colored maps, showing the evolution of the efficiencies for varying pressure ratios and inlet qualities. Those maps have been analyzed checking the influence of the speed and the OCR. The results have shown a decrease in efficiency at low vapor qualities, especially for high pressure ratios, where under-compression is amplified. Generally, when increasing the speed, both volumetric and isentropic efficiencies are increased for low vapor qualities, while the isentropic efficiency decreases for high vapor qualities, certainly due to increased friction. Moreover, the increase of the oil circulation ratio seems to globally increase the performance, by increasing the viscosity of the liquid phase. Finally, the results of the pure-refrigerant compression have been analyzed, showing decent isentropic efficiencies (minimum of 50%) for a given optimal pressure ratio of 2.7. Some explanations have been found to interpret the results; however, a deeper analysis is necessary to confirm the presented tendencies. The validation of a model could help in confirming the analysis. Overall, it seems that leakages management is critical when operating in two-phase and similar tendencies have been found in researches with liquid-flooded screw compressor. Therefore, reducing the leakage gaps by using compliance mechanism could improve the performance of two-phase compression. Finally, increasing the built-in volume ratio would also improve the performance at higher compression ratios.

Data availibility

The experimental data used to generate the results present in this article can be found at the following Zenodo link for the three experimental campaign: Zenodo.

A. Orbiting mechanism of the tested open-drive scroll compressor

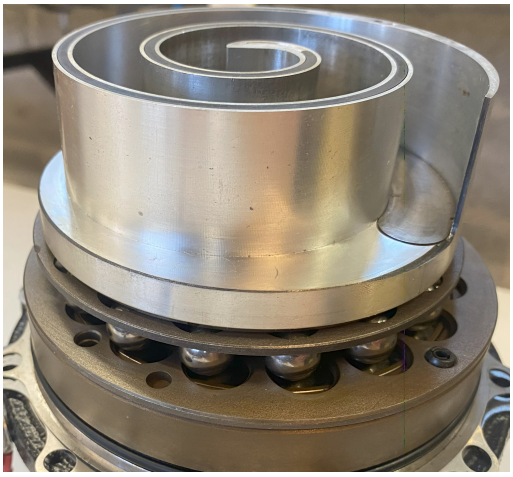

Figure 24: Orbiting mechanism of the tested open-drive scroll compressor (Sanden TGVE08).

B. Test bench picture

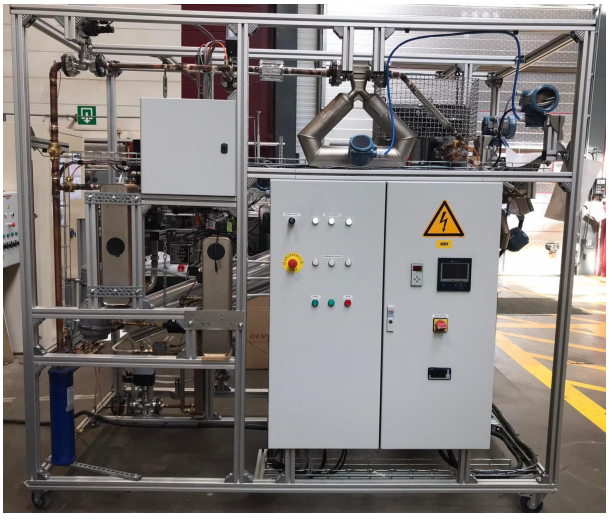

Figure 25: Test bench picture.

C. Cavestri equation and parameters

$$P(x_{\text{ref}}, T) = x_{\text{ref}} P^{\sigma}_{\text{ref}}(T) + x_{\text{ref}} \cdot (1 - x_{\text{ref}}) \cdot (a_1 + a_2 T + a_3 T^2 + a_4 + a_5 x_{\text{ref}} T + a_6 x_{\text{ref}} T^2) \quad (15)$$

Table 3
Empirical parameters of the Cavestri equation both both oil-refrigerant mixtures.

Parameter	Pure oil	Oil mixture
a_1	$-4.81 \cdot 10^{-12}$	$1.05 \cdot 10^{-5}$
a_2	$-3.36 \cdot 10^{-9}$	$1.07 \cdot 10^{-3}$
a_3	$-2.04 \cdot 10^{-6}$	$-7.92 \cdot 10^{-6}$
a_4	$4.18 \cdot 10^{-11}$	$1.05 \cdot 10^{-5}$
a_5	$1.42 \cdot 10^{-8}$	$2.14 \cdot 10^{-3}$
a_6	$4.74 \cdot 10^{-6}$	$3.69 \cdot 10^{-6}$

References

Bell, I.H., Lemort, V., Groll, E.A., Braun, J.E., King, G.B., Horton, W.T., 2012a. Liquid-flooded compression and expansion in scroll machines - part i: Model development. International Journal of Refrigeration 35, 1878–1889. doi:10.1016/j.ijrefrig.2012.07.010.

Bell, I.H., Lemort, V., Groll, E.A., Braun, J.E., King, G.B., Horton, W.T., 2012b. Liquid flooded compression and expansion in scroll machines - part ii: Experimental testing and model validation. International Journal of Refrigeration 35, 1890–1900. doi:10.1016/j.ijrefrig.2012.07.008.

Briola, S., Gabbrielli, R., Baccioli, A., Fino, A., Bischi, A., 2021. Thermo-economic analysis of a novel trigeneration cycle enabled by two-phase machines. Energy 227. doi:10.1016/j.energy.2021.120453.

Bush, J.W., Elson, J.P., 1988. Scroll compressor design criteria for residential air conditioning and heat pump applications, part i: Mechanics, International Compressor Engineering Conference. URL: https://docs.lib.purdue.edu/icec.

Ferreira, C.A., Zamfirescu, C., Zaytsev, D., 2006a. Twin screw oil-free wet compressor for compression-absorption cycle. International Journal of Refrigeration 29, 556–565. doi:10.1016/j.ijrefrig.2005.10.006.

Ferreira, C.A.I., Zaytsev, D., Ferreira, C.A.I., 2002. Experimental compression - resorption heat pump for industrial applications, International Compressor Engineering Conference. URL: http://docs.lib.purdue.edu/iracc/601.

Ferreira, C.A.I., Zaytsev, D., Zamfirescu, C., Ferreira, C.A.I., 2006b. Wet compression of pure refrigerants, International Compressor Engineering Conference. URL: https://docs.lib.purdue.edu/icec.

Gudjonsdottir, V., Ferreira, C.A.I., Goethals, A., 2019. Wet compression model for entropy production minimization. Applied Thermal Engineering 149, 439–447. doi:10.1016/j.applthermaleng.2018.12.065.

Hiwata, A., Iida, N., Futagami, Y., Sawai, K., Ishii, N., 2002. Performance investigation with oil-injection to compression chambers on co2-scroll compressor, International Compressor Engineering Conference. URL: https://docs.lib.purdue.edu/icec/1577.

Honeywell, 2018. A better environment with next-generation solstice zd refrigerant.

Leclercq, N., Bederna, B.G., Lemort, V., 2024. Experimental Testing of a Scroll Compressor with Two-Phase Refrigerant Flows. Springer. pp. 239–250. URL: https://link.springer.com/10.1007/978-3-031-42663-6_19, doi:10.1007/978-3-031-42663-6_19.

Leclercq, N., Vega, J., Lemort, V., 2023. Investigations on a heat pump using two-phase refrigerant compressions, in: 36th International Conference on Efficiency, Cost, Optimization, Simulation and Environmental Impact of Energy Systems (ECOS 2023), ECOS 2023. pp. 804–814. URL: http://www.proceedings.com/069564-0073.html, doi:10.52202/069564-0073.

Ni, D.S., 2008. Scroll-type fluid displacement apparatus with fully compliant floating scrolls.

Nikolov, A., Bruemmer, A., 2014. Influence of water injection on the operating behaviour of screw machines, 9th International Conference on Screw Machines. URL: https://www.researchgate.net/publication/316275891.

Quoilin, S., Schrouff, J., 2016. Assessing steady-state, multivariate experimental data using gaussian processes: The gpexp open-source library. Energies 9, 423. doi:10.3390/en9060423.

Ramaraj, S., Yang, B., Braun, J.E., Groll, E.A., Horton, W.T., 2014. Experimental analysis of oil flooded r410a scroll compressor. International Journal of Refrigeration 46, 185–195. doi:10.1016/j.ijrefrig.2014.08.006.

Sakuda, A., Sawai, K., Lida, N., Hiwata, A., Morimoto, T., 2001. Performance improvement of scroll compressor with new sealing-oil supply mechanism, International Conference on Compressors and their Systems. doi:C591/019/2001.

Scialdone, J.J., Miller, M.K., Montoya, A.F., 1996. Methods of measuring vapor pressures of lubricants with their additives using tga and/or microbalances.

Taft, G.L., 1972. Selection and application of industrial screw compressors, International Compressor Engineering Conference. URL: https://docs.lib.purdue.edu/icec.

Vorster, P., Meyer, J., 2000. Wet compression versus dry compression in heat pumps working with pure refrigerants or non-azeotropic binary mixtures for different heating applications. International Journal of Refrigeration 23, 292–311. URL: https://linkinghub.elsevier.com/retrieve/pii/S014070079900050X, doi:10.1016/S0140-7007(99)00050-X.

Youbi-Idrissi, M., Bonjour, J., 2008. The effect of oil in refrigeration: Current research issues and critical review of thermodynamic aspects. doi:10.1016/j.ijrefrig.2007.09.006.

Zimmern, B., 1984. From water to refrigerant: Twenty years to develop the oil injection-free single screw compressor, International Compressor Engineering Conference. URL: https://docs.lib.purdue.edu/icec.